ACTA ACUSTICA UNITED WITH ACUSTICA
Vol. 96 (2010) 266 – 274

DOI 10.3813/AAA.918276

Vibro-Acoustic Properties of Auxetic Open Cell Foam: Model and Experimental Results

I. Chekkal[1)], M. Bianchi[1)], C. Remillat[1)], F.-X. Bécot[2)], L. Jaouen[2)], F. Scarpa[1)]

[1)] Department of Aerospace Engineering, University of Bristol, Queens Building, BS8 1TR, Bristol, UK.
matteo.bianchi@bris.ac.uk

[2)] MATELYS-Acoustique & Vibrations, 20/24 rue Robert Desnos, 69120 Vaulx-en-Velin, France

Summary

The combined mechanical and acoustic properties of auxetic (negative Poisson's ratio) foams are described both from a numerical and experimental point of view. Samples of open cell PU-PE foams with negative Poisson's ratio are produced using a dedicated manufacturing process, and subjected to tensile quasi static and cyclic loading, as well as sound absorption measurements based on ISO 10-534-2 Standard. A homogenization model based on the Biot's theory is also derived to calculate the poroelastic parameters of the foam. The experimental and numerical results are compared and commented to provide explanations regarding the unusual acoustic absorption of these porous materials.

PACS no. 43.40.+r

1. Introduction

Negative Poisson's ratio (NPR) foams have been manufactured for the first time in 1987, from open cell PU industrial foam using a manufacturing process involving the buckling of the cells and the crystallisation of their deformed shape [1]. Since the publication of that seminal paper, a wide range of materials featuring the NPR effect has been produced, from long fibre composites to honeycombs and microporous polymers [2]. The wave propagation properties of auxetics have been studied from a theoretical [3] and numerical/experimental perspective in deterministic cellular structures [4] and composite materials [5]. In 1994, Howell, Prendergarst and Hansen measured the acoustic absorption of transformed NPR foams [6]. Measurement were also performed by Scarpa et al on auxetic foams with small PR values [7], also doped with MRF (i.e. foam with a magnetorheological (MR) fluid coating) fluid particles [8, 9]. A common aspect for all the auxetic foams tested was the significant increase in terms of acoustic absorption (2–2.5 times) at frequencies below 350 Hz compared to the conventional foam phase from which they were derived. However, it is not clear yet how the microstructure of these foams affects the sound properties of the samples so far produced. Moreover, there have been no formal attempts at this point to model the poroelastic parameters of these unusual foams. In this study, we attempt to correlate the mechanical and acoustic properties of open cell negative Poisson's ratio foams with considerations from the numerical homogenization of the static poroelastic parameters using Biot's theory [10], which is described in this paper in paragraph 2.1.

The theory of linear isotropic poroelasticity was first introduced by Biot in 1941 [10]. Based on symmetry arguments Biot demonstrated the existence of four independent material constants for isotropic poroelasticity and six for in-plane elasticity. Biot then extended the isotropic theory to the anisotropic one in 1955 [11]. However, the physical meaning of these parameters is still obscure due to the lack of laboratory measurements of the anisotropic material constants. A homogenization method is applied to Biot's model in order to define an approximate mathematical model in which the *effective* properties of the medium are computed and which therefore would be suitable for efficient computation [12].Using the obtained poroelastic coefficients, an investigation of the sensitivity of these parameters to changes in the pore geometry for both conventional and auxetic cells can be performed, and therefore, provide a clearer prospect of the contribution of these coefficients to the acoustical properties of auxetic foams.

In the mechanical analysis, specimens were converted from conventional Poisson's ratio into auxetic, and then subjected to tensile and compressive quasi static cyclic loading. The manufacturing route adopted involved a biaxial compression of the original foam, heating of the compressed specimens above the T_g (glass transition temperature) of the foam polymer, and cooling under running water. A specific compression ratio was used to convert the sample and a final temperature of 135 °C was chosen. Tensile and compressive cyclic tests were performed in order to measure tangent modulus, Poisson's ratios and energy dissipated per unit volume. The sound absorption proper-

Received 20 May 2009,
accepted 15 January 2010.

ties have been measured in an impedance tube according to ISO Standard [13, 23].

2. Modelling

2.1. Poroelastic Parameters

To describe the propagation of the sound waves inside air saturated porous materials while accounting for the skeleton deformation, a widely used model has been proposed by Biot [14]. Biot's relations for anisotropic materials can be written as

$$\begin{aligned} \sigma_{ij} &= M_{ijkl}e_{kl} - \alpha_{ij}P, \\ P &= M(\zeta - \alpha_{ij}e_{ij}), \end{aligned} \tag{1a}$$

$$\begin{aligned} \mathrm{div}(\sigma) &= \frac{\partial^2}{\partial t^2}\left(\rho_{11}u + \rho_{12}U\right) + b\frac{\partial}{\partial t}\left(u - U\right), \\ \mathrm{grad}(P) &= \frac{\partial^2}{\partial t^2}\left(\rho_{12}u + \rho_{22}U\right) - b\frac{\partial}{\partial t}\left(u - U\right), \end{aligned} \tag{1b}$$

$$\begin{aligned} \rho_1 &= (1-\phi)\rho_s, \quad \rho_2 = \phi\rho_f, \quad \rho_{12} = -\rho_a, \\ \rho_{11} &= \rho_1 + \rho_a, \quad \rho_{22} = \rho_2 + \rho_a, \end{aligned} \tag{1c}$$

where σ_{ij} is the total stress tensor, e_{ij} is the total strain tensor, P is the pore pressure and ζ is the fluid content variation, representing the rate of change of volumetric fluid content in the pore. M_{ijkl}, α_{ij} and M are the constitutive poroelastic constants. Equation (1a) is the constitutive stress strain equation for a uniform porous material and is the main equation used to identify the poroelastic properties in the hydrostatic case. Equation (1b) describes the dynamic behaviour of the foam where u is the solid phase displacement, U is the fluid phase displacement and b is the dissipation factor. Equation (1c) provides expressions for the parameters ρ_{11}, ρ_{12} and ρ_{22} which represent the mass coefficients that account for the effects of momentum transfer between the solid and the fluid phases resulting from the pore tortuosity where ϕ is the porosity, ρ_s is the solid density and ρ_a is the coupling density. In his model, Biot defines porous materials as homogenous, two-phase mixture. In this aspect, Biot's model can be considered as a homogenised model of a structure which contains both a fluid phase and a solid phase. Therefore, the approach used in this study is to obtain Biot's parameters using a homogenisation approach, for which it is important to define a representative volume unit. The three-dimension rectangular truss structure is often used to represent the global mechanical and dynamic properties of open cell foams [15, 16]. However, the rectangular topology does not allow representing the complexity of a conventional and auxetic foam unit cell, and therefore more elaborated geometries have to be considered. Simple honeycomb cells were modelled in order to obtain the main parameters related to the properties of auxetic foams. A honeycomb cell is a good representation of a conventional porous foam cell, providing the cross-section of a tetrakaidecahedron [17]. The importance of the unit cell geometry over the transport properties of foams has been also assessed with coupled CFD- FE models of open Kelvin lattices to simulate the equivalent permeability of the porous material [18]. The hexagonal (centre-symmetric) cells used in this work have a regular geometry. Therefore, it is possible to evaluate the mechanical deformations and overall properties of these regular cellular structures with closed analytical solutions [15], or other homogenisation techniques [18]. Assuming periodic and symmetric cell geometry, the model is then simplified to a quarter of a cell. In the case of orthotropic materials with two mutually orthogonal planes of elastic symmetry, there exist nine independent material coefficients (six M_{ij}, two α_{ij} and one M). Equations (1a) reduce to

$$\begin{aligned} \sigma_{xx} &= M_{11}e_{xx} + M_{12}e_{yy} - \alpha_{xx}P, \\ \sigma_{yy} &= M_{12}e_{xx} + M_{22}e_{yy} - \alpha_{yy}P, \\ \sigma_{zz} &= M_{13}e_{xx} + M_{23}e_{yy}, \\ \sigma_{xy} &= M_{66}e_{xy}, \end{aligned} \tag{2}$$

$$P = M\zeta - \alpha_{xx}e_{xx}M - \alpha_{yy}e_{yy}M. \tag{3}$$

M_{11}, M_{12}, M_{22}, M_{13}, M_{23}, M_{66}, M, α_{xx} and α_{yy} are the poroelastic parameters [19].

In this paper, the hydrostatic behaviour of auxetic foams will be investigated by identifying the poroelastic parameters in the constitutive stress train relations described in Equation (1a). The dynamic properties which are related to the fluid viscosity, the shape of the cell and the coupling between the motion of the fluid and the solid phases will be investigated in further studies. A plain strain 2D finite element analysis of open cell porous foam has been conducted in the hydrostatic case. The finite element modelling was performed using embedded COMSOL-MATLAB software (COMSOL MULTIPHYSICS with MATLAB). The software enables the user to define the cell geometry, apply appropriate boundary conditions and establish the set of partial differential equations for the problem, which are solved using the finite element discretisation of the problem domain. The re-entrant structure of the hexagonal cell can be simplified into figure 1 by using periodic boundary conditions. Due to symmetry, the re-entrant unit cell can be simplified to a quarter of a unit cell. The foam cells were modelled starting from a parametric template with the geometric non-dimensional parameters: the wall aspect ratio α (h/l), the relative density β (t/l), and internal cell angle θ [20]. In the case of re-entrant auxetic cells, a limiting geometric condition was defined by the minimum allowed internal cell angle to avoid the contact of the opposite vertices [20], as shown in Figure 1. In this case, the limiting condition for two-phase composite foams is

$$\theta_{\mathrm{lim}} = \frac{\pi}{2} - \cos^{-1}\left(\frac{\alpha}{2} - \frac{\beta}{2\sin\phi}\right). \tag{4}$$

The cell was modelled in a plain strain condition as the auxetic media is assumed to have infinite pore length with finite thickness. In the hydrostatic case, the variation of the fluid pressure in the pores was assumed to be constant; hence, the fluid in the pores was modelled as a void as no

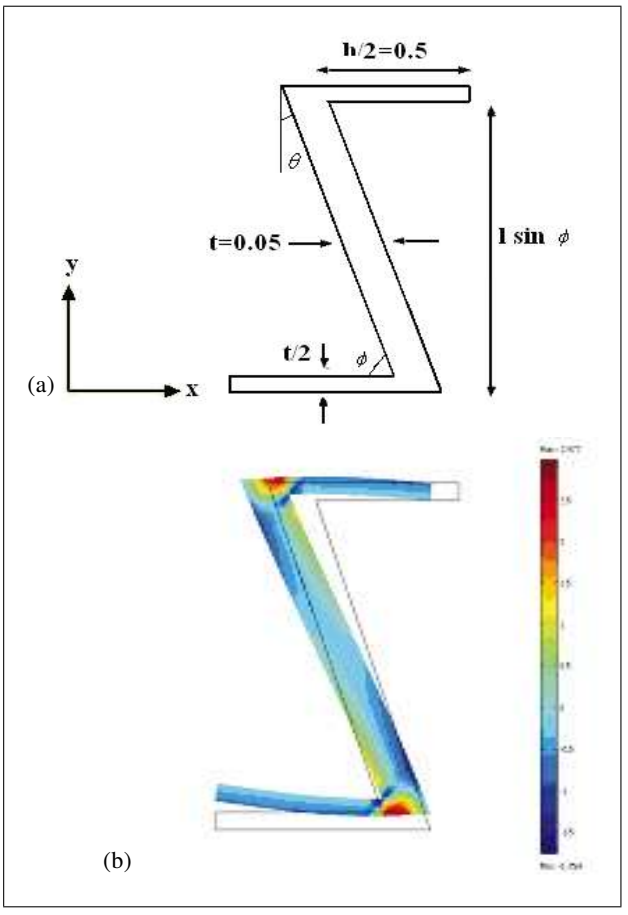

Figure 1. Auxetic cell geometric dimensions (a) and the resulting deformation of an imposed pure shear strain (b).

mesh is needed. A quarter of the unit cell was modelled and three in-plane loading cases (e_{xx}, e_{yy}, e_{zz}) were imposed on the model. Results obtained from the computed models are then used in the poroelastic parameters calculations. Using Green's theorem, The homogenised values of Biot's parameters can be obtained averaging stresses and strains.

First, a uniaxial displacement in the x direction is applied assuming no pore pressure variation. Hence equation (3) results in

$$\begin{aligned} \langle \sigma_{xx} \rangle &= M_{11} \langle e_{xx} \rangle, \qquad \langle \sigma_{yy} \rangle = M_{12} \langle e_{xx} \rangle, \\ \langle \sigma_{zz} \rangle &= M_{13} \langle e_{xx} \rangle. \end{aligned} \tag{5}$$

The fluid content variation can be expressed as [14]

$$\zeta = \phi \operatorname{div} \left(\mathrm{e}_p \right) + \phi C_f P, \tag{6}$$

where C_f (the fluid compressibility) is defined as $C_f = -(1/\rho_0)(\partial\rho/\partial P)$. Hence,

$$\zeta = \phi \operatorname{div} \left(\mathrm{e}_p \right). \tag{7}$$

Assuming no fluid pressure variation, equation (1a) becomes

$$P = M\zeta - \alpha_{xx} e_{xx} M = 0. \tag{8}$$

Therefore,

$$\zeta = \alpha_{xx} \langle e_{xx} \rangle. \tag{9}$$

Similarly to the above, a uniaxial displacement in the Y direction is applied assuming no pore pressure variation. Hence equation (2, equilibrium along the y-direction) results in the following

$$\begin{aligned} M_{12} &= \frac{\langle \sigma_{xx} \rangle}{\langle e_{xx} \rangle}, \qquad M_{22} = \frac{\langle \sigma_{yy} \rangle}{\langle e_{yy} \rangle}, \\ M_{23} &= \frac{\langle \sigma_{zz} \rangle}{\langle e_{yy} \rangle}. \end{aligned} \tag{10}$$

Similarly, to the first case, an expression for α_{yy} can be obtained,

$$\alpha_{yy} = \frac{\zeta}{\langle e_{yy} \rangle}. \tag{11}$$

By applying a pure shear displacement to the cell, assuming no pore pressure variation, an expression for the stress can be written as

$$\langle \sigma_{xy} \rangle = M_{66} \langle e_{xy} \rangle. \tag{12}$$

In order to determine the poroelastic fluid dependent parameter M, the cell frame was assumed to be rigid: $e^s_{ij} = 0$. This is a realistic assumption since the poroelastic coefficient M is representative to the fluid compressibility. No strain in the skeleton results in no strain in the pores as the interactive skeleton fluid boundary is fixed.

The total strain is defined as

$$e_{ij} = (1 - \phi) e^S_{ij} + \phi e^P_{ij} \tag{13}$$

Since

$$e^S_{ij} = e^P_{ij} = 0, \quad e_{ij} = 0. \tag{14}$$

The above assumption results in

$$P = M\zeta - M a_{ij} e_{ij} = M\zeta. \tag{15}$$

The fluid content variation defined in equation (6) reduces to

$$\zeta = \phi \operatorname{div} \left(e_p \right) + \phi C_f P = \phi C_f P. \tag{16}$$

Hence,

$$P = M \phi C_f P. \tag{17}$$

The fluid in the modeled cells is assumed to be a perfect gas, which results in

$$M = 1/\phi. \tag{18}$$

Biot's hydrostatic poroelastic parameters can be obtained for different cell geometries including conventional and auxetic cells.

3. Manufacturing and testing

3.1. Mechanical testing

The original material used was a conventional open-cell PU based foams with 27 kg/m^3 density. Cylindrical specimens of 58 mm initial diameter and 65 mm of initial length were cut from a block of conventional foam by using a hot wire cutter device. The conversion process applied to the foams was similar to that of [21] and [22]. The mould used during the process consists of a metallic tube with two calibrated discs sliding inside. The correct position on the discs was assured by a mechanic clamp. The axial and radial compression ratios of 1.5 and 1.3 respectively were defined depending on the radial dimension of the tube and the predefined length of the clamp's edges. A specific time-temperature profile was applied to the sample constrained into the mould during the conversion up to the final temperature of 135 °C. Following the heating stage, the specimen in the constrained status inside the mould was cooled down under running ambient water and relaxed by manually stretching. Prior to testing, both ends of the specimen were cut because of the residual stress. Details of the specimens and the processing are given in Table I and Table II. The specimens were placed close to a radiator for a few hours in order to dry completely. Measurements of dimensions and mass of the specimen were performed one week after the conversion obtaining steady results [21]. An electronic scale (±0.001 g) and a gauge (±0.01 mm) were used to the scope and the results were averaged to obtain mean values of diameters. The density of the conventional foam, ρ_{conv} was 27 kg/m^3. The final density, ρ, of the specimens was measured and the Final Density Ratio FDR was calculated as

$$FDR = \rho/\rho_{\text{conv}}. \tag{19}$$

A 10 kN Shimadzu Autograph AGS testing machine equipped with a 50 N load cell was used for the tensile and compressive mechanical characterisation of both conventional and auxetic specimens. The tests were performed in a quasi-static cyclical mode at a frequency of 0.03 Hz from a just relaxed position up to the 10% of strain. An optical system videoextensometer was used to measure longitudinal and radial deformations by capturing length data in the central part of the specimens closed off by using temporary black surface markers [22]. Values of force, length and width in the strain rate were obtained and a linear stress-strain behaviour was found in the specimens.

The longitudinal (z) and radial (r) strains, Poisson's ratio, tangent modulus and energy dissipation (hysteresis area) where calculated. The Poisson's ratio ν_{zr} was calculated as the negative ratio between the radial and longitudinal strains using a best fit to the strain-strain graph,

$$\nu_{zr} = -\varepsilon_r/\varepsilon_z. \tag{20}$$

Since the linear stress-strain response of such samples is known to remain up to 25% strain in both conventional and auxetic foam [22], values of tangent modulus, E, was calculated as the best fit slope of the linear region of the stress-strain curve between 0 and 10% longitudinal strain,

$$E_z = \mathrm{d}\sigma_z/\mathrm{d}\varepsilon_z. \tag{21}$$

Finally the dissipation of energy in each specimen was calculated from the hysteresis area in the force-deflection data by approximating the sides of each force-deflection curve with two second degree polynomial curves

Table I. Description of the geometry of the samples of conventional Foam.

Length	Diameter	Density
65 mm	58 mm	27 kg/m^3

Table II. Details of the conversion parameters adopted in the conversion into auxetic. C_L and C_T: Longitudinal and transversal compressive ratio; T_f: Final temperature; t: Time.

C_L	C_T	T_f	t	Cooling
1.5	1.3	135 °C	15 min	Water

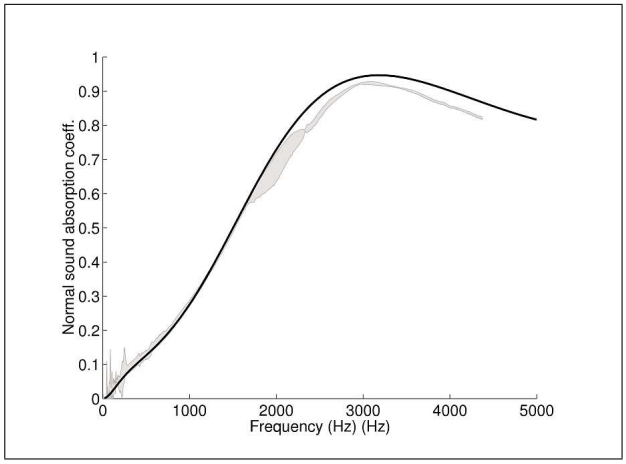

Figure 2. Normal incidence sound absorption coefficients for conventional foam samples of thickness 21.5 mm. Dispersion on measurements (grey area), simulation with parameters reported at Table V (black line). Ambient conditions of temperature and pressure.

3.2. Acoustic testing

To study the effects of the manufacturing process on the sound propagation in auxetic materials, normal sound absorption measurements have been performed on 46 mm-diameter samples of conventional and auxetic foams following the procedure of the corresponding ISO standard [23].

Figure 2 presents the normal incidence sound absorption results for conventional foam samples of thickness 21.5 mm. The grey area represents the dispersion between measurements on both sides of two different samples, which means a total of four measurement data. The low dispersion between these measurements reveals the homogeneity of the foam among the specimen tested. It also

shows that the tested samples have symmetrical properties along their thicknesses, which however does not exclude the existence of a property gradient in the material thickness. This latter aspect was not investigated in the present study.

Figure 3 presents the normal sound absorption coefficients of an auxetic sample of 26 mm. The grey area represents here the dispersion between the measurement results of the two sides of the samples. The low level of dispersion reveals a good homogeneity of the auxetic foam in the thickness, as further discussed and demonstrated in paragraph 4.2.

The comparison of the absorption measurements of the conventional and of the auxetic foams shows that the applied process changes significantly the acoustic properties of the foam. The resulting auxetic foam has larger absorption properties in the low frequency range, below approximately 1500 Hz. In this frequency range, the absorption of the auxetic foam reaches 0.6 at 500 Hz. At higher frequencies, the absorption coefficient of the auxetic sample reaches a plateau which does not exceed 0.7 compared to the maximum of absorption of the conventional foam which reaches almost 100% of absorption around 2500 Hz. In total, the absorption level of the auxetic foam is almost constant from 500 Hz to 4500 Hz, i.e. the highest measured frequency observed here. The dissipation mechanisms will be further discussed in the next section.

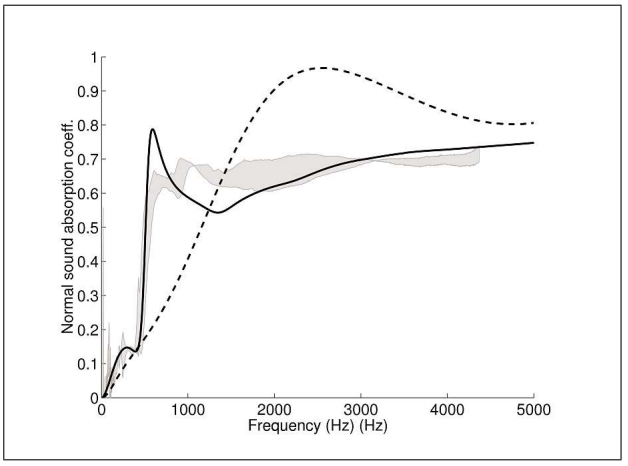

Figure 3. Normal incidence sound absorption coefficients of auxetic foam samples of thickness 26 mm (grey area). Dispersion on measurements (grey area), simulation for the auxetic sample (black line), simulation for the conventional foam (dotted line). Simulations obtained using the parameters of Table V. Ambient conditions of temperature and pressure.

4. Results and discussion

4.1. Mechanical properties

As a benchmark of the Finite Element homogenisation procedure used in this work, the strain-energy based homogenisation technique proposed by Odegard [18] has been applied to compare the elastic coefficient M_{ij} on a reentrant cell (reference core material properties = 26.7 Pa, Poisson's ratio: $\nu_s = 0.33$, :internal angle $\theta = -20°$ and $h = l = 1$ m). The coefficients M_{11}, M_{12} and M_{66} calculated with the present homogenisation technique were 0.24, −0.8 and 0.016 respectively. The strain-energy based technique was providing for the same quantities values equal to 0.23, −0.93 and 0.013, with maximum percentage error of 13% for the coefficient M_{12}. It is worth noticing that the homogenisation technique correctly predicts the negative values of the coefficient M_{12} for auxetic configurations [20]. It is also worth noticing that the coefficients M_{ij} can be represented as the product of the Young's modulus of the core material E_c for a factor describing the geometric layout of the cell: $M_{ij} \approx E_c \overline{M}_{ij}$ [17, 15, 20].

The calculations of the poroelastic coefficients were performed on a honeycomb cell with the following geometric properties: internal angle $\theta = 20°$ and for the conventional case and $\theta = -20°$ for the auxetic cell and the following materials properties; Young's modulus: $E_s = 26.7$ Pa and Poisson's ratio: $\nu_s = 0.33$. Hence, the hydrostatic poroelastic parameters obtained are represented in Table III. Figure 1 represents the auxetic cell geometric

Table III. Hydrostatic Poroelastic Parameters for both Conventional and Auxetic cells.

	Conventional Cell	Auxetic Cell
M_{11} [N/m^2]	0.39	0.24
M_{12} [N/m^2]	0.63	−0.80
M_{13} [N/m^2]	0.34	−0.19
M_{22} [N/m^2]	1.03	3.23
M_{23} [N/m^2]	0.54	0.80
M_{66} [N/m^2]	0.07	0.02
α_{xx}	1.04	0.95
α_{yy}	0.27	0.21
M	1.11	1.31

dimensions and the resulting deformation of an imposed pure shear strain. In addition, the geometry of the honeycomb cell was changed within limitations as a function of θ. The resulting hydrostatic poroelastic parameters were then plotted against the variation in Poisson's ratio to compare between auxetic and conventional foams as illustrated in Figure 4. The inverted hexagonal cell layout is similar to the one of the auxetic foams, where the convex cell shape is provided by the buckling of the cell ribs during the axial compression in mold [1].

By comparing the poroelastic coefficients obtained for both conventional and auxetic cells using the same geometric constants ($h = l = 1$ m), it can be noticed that the elastic parameters M_{12} and M_{13} have a negative sign in auxetic cells compared to the conventional honeycomb cell. On the other hand, it can be observed that the coupling terms α_{xx} and α_{yy} have higher values in the conventional case than that of the auxetic one.

The variation of the elastic parameters with Poisson's ratio is expected. It is due to the fact that the elastic coefficients M_{ijkl} are a function of both Poisson's ratio and Young's modulus. On the other hand, the parameter of in-

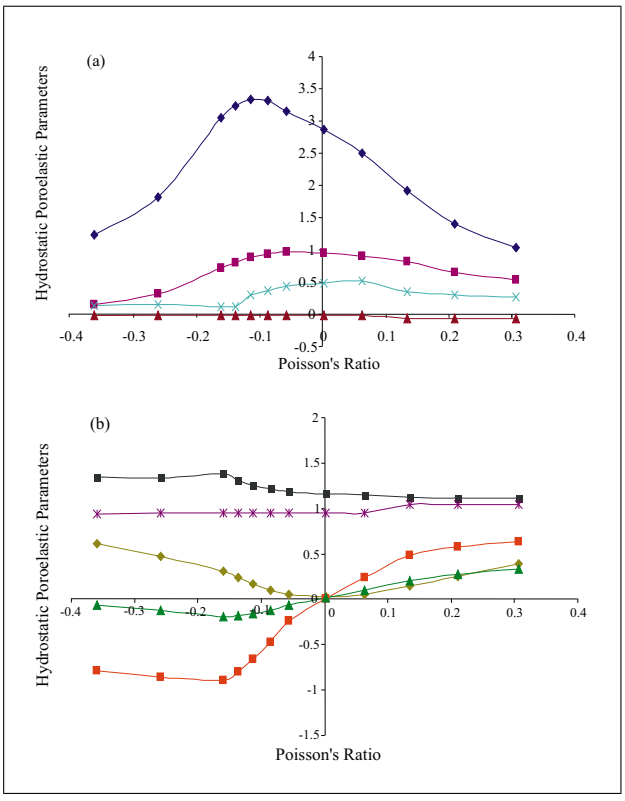

Figure 4. Variation of hydrostatic poroelastic parameters M_{22}, M_{23}, M_{66} and α_{yy} (a) and M_{11}, M_{12}, M_{13}, M and α_{xx} (b) versus Poisson's ratio. The parameters M_{ij} are expressed in N/m^2 whereas α_{xx}, α_{yy} and M are non dimensional parameters.

Table IV. Mean results from quasi-static concerning both auxetic and conventional specimens. ρ: Density [kg/m^3], ν: Poissosn ratio, ElMod: Elastic Modulus [Mpa], Ediss: Energy dissipation [mJ/cm^3].

	ρ	ν	ElMod	Ediss
	Auxetic samples			
Compressive type	89	-0.09	0.02	0.04
Tensile type	89	-0.09	0.02	0.03
	Conventional samples			
Compressive type	27	0.27	0.09	0.22
Tensile type	27	0.47	0.17	0.66

terest in this study is the coupling parameter, where it can be noticed that there is a higher coupling effect in conventional foams compared to auxetic ones. From the FE simulations, no distinctive variation in the coupling terms with increasing Poisson's ratio values from negative (i.e. auxetic) to positive (i.e. conventional) has been observed. Such trend would lead to the initial conclusion that the coupling terms are hardly sensitive to changes in the pore geometry in the hydrostatic case.

Samples of conventional and auxetic foams were prepared and then tested to analyze them both mechanically and acoustically. Figures 5a and 5b show an example of stress-strain curve of the same tested both under tensile

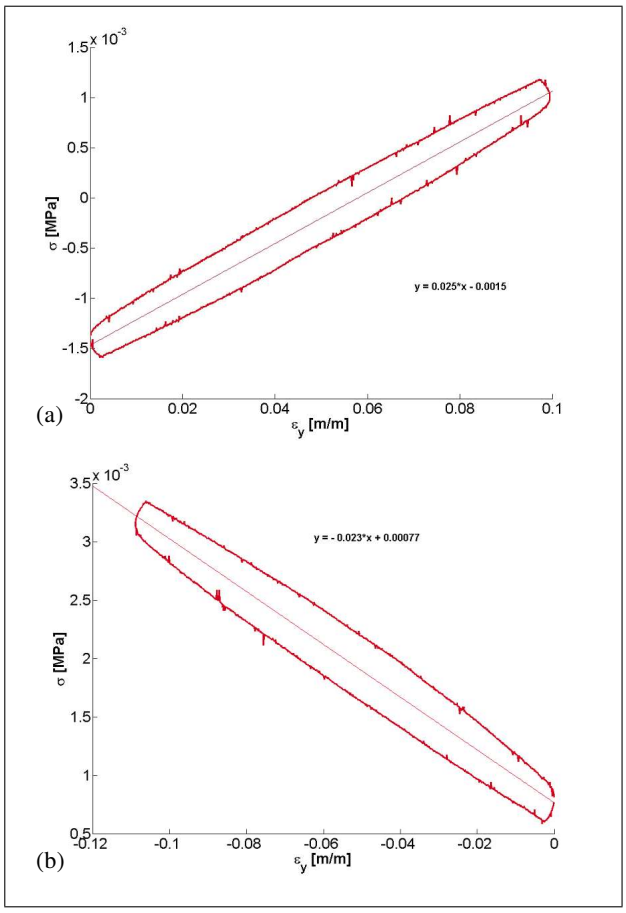

Figure 5. Stress-strain curve gathered from tensile (a) and compressive (b) quasi static cyclic test on auxetic PU based open-cell foam.

(a) and compressive (b) loading. The complex stiffness (storage modulus) and loss factor were derived from the hysteresis loops following the method outlined in [22]. Equations describing the best fit line are illustrated in both figures showing the value of elastic modulus as the slope of the curve. Table IV summarises the mean results of quasi-static tests carried out on samples made specifically to fit inside the impedance tube for the acoustic tests. Mean values of Poisson's ratio of -0.09, elastic modulus of 0.02 MPa and energy dissipation of 0.03 mJ/cm^3 were found in the sample both under compressive and tensile loading. A mean value of 3.3 was also found as FDR. In a previous work made by two of the authors [22], it was found that the compression imposed to the sample represent the most significant parameter in the conversion process of conventional foams. Samples of the conventional foam were also tested following the same procedure used for the auxetic ones. The mean results are illustrated in Table IV. Remarkable differences were found between the conventional and auxetic samples. The conventional foams show positive values of Poisson's ratio and average higher elastic modulus and energy dissipation results than the auxetic ones. It is also of interest to underline that the homogenisation technique provides an overall agreement with the experimental values for the auxetic foam, in par-

ticular for what concerns the Young's modulus. For a core polyurethane material with Young's modulus of 1300 kPa [15], the uniaxial stiffness for the auxetic foams can be expressed by the poroelastic parameter M_{11}, being equal to 12 kPa, while the experimental value is close to 20 kPa (Table IV). The Poisson's ratio from the homogenisation simulation ($\sim M_{12}/M_{22}$ [15]) is higher compared to the experimental value (-0.24 against -0.10). However, the Poisson's ratio is very sensitive to the internal cell angle and aspect ratio layout, and small changes of θ lead to significant changes of the in-plane Poisson's ratios, with factors from 4 to 5 [20].

4.2. Acoustic parameters

To go deeper in the description of visco-thermal dissipative phenomena which occur in these materials, complete parameter characterisations have been carried out. The low dispersions observed on the measured acoustic absorption coefficients shown in Figures 2 and 3 show that the sets of data are appropriate for the characterization. The procedure proposed here is based on the technique described by Olny and his colleagues in [24, 25, 26] which requires the prior knowledge of the static air flow resistivity and of the open porosity of the material. These two latter quantities were directly measured on dedicated experimental rigs using the corresponding ISO 9053 standard [13] for the air flow resistivity and the method proposed by Beranek in [27], and further refined by Champoux [28] in the absence of a standard for this type of measurement. The characterization is then carried out from the measured values of the dynamic mass density and bulk compressibility. From this set of data, the values of the parameter of the Johnson-Champoux- Allard-Lafarge model [29, 30, 31] are determined and reported in Table V for both the conventional and the auxetic foam.

The values obtained for the conventional foam are typical of low air flow resistivity polymeric foam. From the definitions of these parameters, one can notice large pore size and relatively small size of inter-connections between the pores. Finally, as shown in Figure 2, the simulated normal sound absorption coefficient obtained with these parameters present a good correspondence between measurements and simulation can be observed under 1800 Hz. Above this frequency, motions of the porous frame noticeably influence the sound absorption. These frame motions are not accounted for in the simulation and partly explain the differences observed between measurements and simulation in the frequency range [2000–5000] Hz.

The measured value of the static air flow resistivity for the auxetic foam reported in Table V shows an important increase compared to that of the conventional foam. Given the order of magnitude of resistivities for conventional and auxetic materials, the absorption coefficient for the auxetic foam is expected to be higher, respectively lower, in the low frequency range, respectively high frequency range, compared to the absorption level of the conventional foam which is less resistive. The absorption coefficients reported in Figure 3 confirm these tendencies and are in accordance

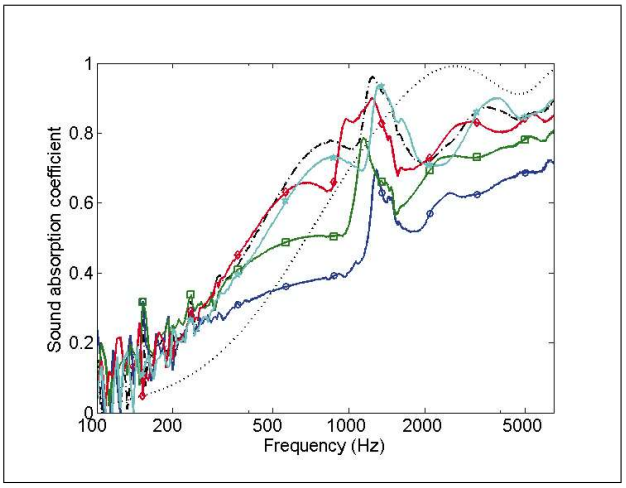

Figure 6. Normal incidence sound absorption coefficients of auxetic foam samples of thickness 35 mm obtained using various parameters for the transformation process (circles, square, diamond, star). Measurements for the non-auxetic foam of thickness 39 mm (black dash-dotted line), Simulation of a Melamine foam sample of thickness 35 mm (black dotted line). Ambient conditions of temperature and pressure.

with the measured value of the air flow resistivities. For the auxetic foam, the characterisation has been carried out in frequency regions where the influence of the frame deformation is low, namely in the low frequency range below 500 Hz and at high frequencies above 2 500 Hz (see the dotted curve with circles in Figure 3). However, as recommended by the value of the FAE criterion presented in [32], the sound absorption coefficient of the auxetic sample has been computed accounting for the frame deformation (see black full line) with the value of the elastic parameters reported in Table IV. It is observed in Figure 3 that this model allows to capture the general behaviour of the measured sound absorption coefficient on most of the frequency range. The sharp dip around 500 Hz is due to a quarter wave length resonance in the porous thickness (the estimated theoretical value is 456 Hz) and largely depends on the actual value of the structural loss factor of the sample in the tube. In the high frequency range, deviations may be due to a bad fit of the sample inside the tube.

Figure 6 presents the sound absorption coefficient measured for several auxetic samples of thickness 35 mm obtained with various manufacturing parameters. Measurement results are compared to the sound absorption coefficients measured for the original foam used to apply the auxetic process, only available however for a 39 mm thickness. This increased thickness is in favour to the auxetic samples in the low frequency range. Also reported is the sound absorption coefficient simulated for a sample of Melamine foam of the same thickness than auxetic samples (see for instance [33] for the Melamine parameters). The comparison of performances in the low frequency range show that it is possible to obtain an auxetic foam, i.e. with improved elastic and damping performances, with, at

Table V. Acoustic parameters of conventional and auxetic foams. Values in parenthesis are standard deviation on the measurement data. σ: static air flow resistivity [Ns/m^4], ϕ: open porosity, α_∞: high frequency limit of tortuosity, Λ: viscous characteristic length [µm], Λ': thermal characteristic length [µm], k_0': static thermal permeability [10^{-10}m].

	σ	ϕ	α_∞	Λ	Λ'	k_0'
Conventional foam	12500 (100)	0.98 (0.01)	1.25 (0.04)	61 (1)	327 (52)	104 (4)
Auxetic foam	194300 (300)	0.94 (0.01)	1.55 (0.31)	10 (2)	61 (1)	82 (8)

least, equal absorption properties compared to foams obtained using a more conventional manufacturing process.

It is important to note that the measurements on others auxetic foam materials (obtained with different manufacturing parameters and which are not shown here for the sake of concision) show that it is possible to obtain auxetic foam with, at least, equal absorption properties than a given conventional foam for an equal thickness of materials.

5. Conclusions

The sensitivity of the poroelastic parameters to changes in the pore geometry has been investigated. Results showed that the coupling terms in the positive poison's ratio range representing conventional cells, are higher than those in the negative Poisson's ratio range which represents auxetic cells. The variation in elastic terms was expected as the elastic coefficients M_{ijkl} are a function of Young's modulus and Poisson's ratio. Furthermore, increasing Poisson's ratio values from negative to positive did not have a strong effect on the coupling terms as they showed a relatively stable tendency. Such trend would lead to the initial conclusion that the coupling terms are not sensitive to changes in the pore geometry in the hydrostatic case. Also auxetic samples show a different mechanical and acoustic behaviour compared to conventional ones. At the peculiar testing conditions the conventional samples present higher values of stiffness and energy dissipation as opposed to auxetic ones.

At low frequencies up to 1500 Hz, auxetic foams show enhanced acoustic absorption properties compared to conventional one whereas plateau behaviour is observed in the range of 1000–4000 Hz. On the other hand, the mechanical properties (resilience and unusual deformation mechanism), as well as the high sound absorption compared to conventional porous materials have been further validated, in the case of NPR close to -0.10. Our experience shows that auxetic foam samples have higher static air flow resistivity compared to the conventional foam samples from which they are derived. The extent of this increase depends on the manufacturing parameters and will be further investigated by building up a model linking the geometric microstructural properties to the acoustic macroscopic parameters. Finally, it may be underlined that the acoustic model assumes that the material is isotropic even though the elementary cell chosen above for the elastic model reveals an apparent orthotropic behaviour. However, the influence of the possible anisotropy on the sound absorption measured and predicted is expected to be low for a plane wave excitation under normal incidence [34].

References

[1] R. S. Lakes: Foam structures with a negative Poisson's ratio. Science **235** (1987) 1038–1040.

[2] W. Yang, Z.-M. Li, W. Shi, B.-H. Xie, M.-B. Yang: On auxetic materials. J. Mat. Sci. **39** (2004) 3269–3274.

[3] A. W. Lipsett, A. I. Beltzer: Reexamination of dynamic problems of elasticity for negative Poisson's ratio. J. Acoust. Soc. Am. **84** (1988) 2179–2186.

[4] A. Spadoni, M. Ruzzene, F. Scarpa: Dynamic response of chiral truss-core assemblies. J. Int. Mat. Syst. Struct. **17** (2006) 941–952.

[5] F. Scarpa, P. G. Malischewsky: Some new considerations concerning the Rayleigh-wave velocity in auxetic materials. Physica Stat. Solidi B **245** (2008) 578–583.

[6] B. Howell, P. Prendergast, L. Hansen: Examination of acoustic behavior of negative Poisson's ratio materials. App. Acoust. **43** (1994) 141–148.

[7] F. Scarpa, L. G. Ciffo, J. R. Yates: Dynamic properties of high structural integrity auxetic open cell foam. Smart Materials and Structures **13** (2004) 49–56.

[8] F. Scarpa, F. C. Smith: Passive and MR fluid-coated auxetic PU foam. Mechanical, acoustic, and electromagnetic properties. Journal of Intelligent Material Systems and Structures **15** (2004) 973–979.

[9] F. Scarpa, W. A. Bullough: Lumley trends in acoustic properties of iron particle seeded auxetic polyurethane foam P. Proceedings of the Institution of Mechanical Engineers, Part C: Journal of Mechanical Engineering Science **218** (2004) 241–244.

[10] M. A. Biot: A general theory of three dimensional consolidation. J. Appl. Phys. **12** (1941) 155–164.

[11] M. A. Biot: Theory of elasticity and consolidation for a porous anisotropic solid. J. Appl. Phys. **26** (1955) 182–185.

[12] A. Bermúdez de Castro, J. L. Ferrín, A. Mikeliæ: Numerical computation of the acoustic properties of porous media obtained by homogenisation techniques. University of Claude Bernard.

[13] ISO 9053: Acoustics. Materials for acoustical applications. Determination for airflow resistance. International Organization for Standardization, 1991.

[14] M. A. Biot: Mechanics of deformation and acoustic propagation in porous media. J. Appl. Phys. **27** (1961) 240–253.

[15] L. J. Gibson, M. F. Ashby: Cellular solids, structure and properties. 2nd edition.

[16] W. N. Patten, S. Shao, C. Mo: A vibration model of open celled polyurethane foam automotive seat cushions. J. Sound Vib. **217** (1998) 145–161.

[17] J. B. Choi, R. Lakes: Analysis of elastic modulus of conventional foams and re-entrant foam materials with negative Poisson's ratio. Int. J. Mech. Sci. **37** (1995) 51.

[18] G. M. Odegard: Constitutive modeling of piezoelectric polymer composites. Acta Materialia **52** (2004) 5315–5330.

[19] M. A. Biot: The theory of propagation of elastic waves in a fluid saturated porous solid. J. Acoust. Soc. Am. **28** (1956) 168–191.

[20] F. Scarpa, C. Remillat, P. Landi, G. Tomlinson: Damping modelization of auxetic foams. Smart Structures and Materials 2000, Damping and Isolation, 2000, 336–343.

[21] F. Scarpa, P. Pastorino, A. Garelli, S. Patsias, M. Ruzzene. Physica Status Solidi B **242** (2005) 681.

[22] M. Bianchi, F. Scarpa, C. W. Smith: Stiffness and energy dissipation in polyurethane auxetic foams. J. Mat. Sci. **43** (2008) 2461.

[23] ISO 10354-2: Acoustics. Determination of sound absorption coefficient and impedance in impedance tubes. Part 2: Transfer-function method. International Organization for Standardization, 1998.

[24] X. Olny, R. Panneton, J. Tran-Van: An indirect method for determining intrinsic parameters of porous materials. – In: Poromechanics II. Auriault et al. (eds.). Swets & Zeitlinger, Lisse, 2002.

[25] R. Panneton, X. Olny: Acoustic determination of the parameters governing viscous dissipation in porous media. J. Acoust. Soc. Am. **119** (2006) 2027–2040.

[26] X. Olny, R. Panneton: Acoustic determination of the parameters governing thermal dissipation in porous media. J. Acoust. Soc. Am. **123** (2008) 814–824.

[27] L. Beranek: Acoustic impedance of porous material. J. Acoust. Soc. Am. **13** (1942) 248–260.

[28] Y. Champoux, M. R. Stinson, G. A. Daigle: Air-based system for the measurement of porosity. J. Acoust. Soc. Am. **89** (1991) 910–916.

[29] D. L. Johnson, J. Koplik, R. Dashen: Theory of dynamic permeability and tortuosity in fluid-saturated porous media. J. Fluid Mech. **176** (1987) 379–402.

[30] Y. Champoux, J.-F. Allard.: Dynamic tortuosity and bulk modulus in air-saturated porous media. J. Appl. Phys. **70** (1991) 1975–1979.

[31] D. Lafarge, P. Lemarinier, J.-F. Allard, V. Tarnow: Dynamic compressibility of air in porous structures at audible frequencies. J. Acoust. Soc. Am. **102** (1997) 1995–2006.

[32] D. Pilon, R. Panneton, F. Sgard: Behavioral criterion quantifying the edge-constrained effects on foams in standing wave tube. J. Acoust. Soc. Am. **114** (2003) 1980–1987.

[33] F.-X. Bécot, L. Jaouen, E. Gourdon: Applications of the dual porosity theory to irregularly shaped porous materials. Acta Acustica united with Acustica **94** (2008) 715–724.

[34] P. Khurana, L. Boeckx, W. Lauriks, P. Leclaire, O. Dazel, J.-F. Allard: A description of transversely isotropic sound absorbing porous materials by transfer matrices. J. Acoust. Soc. Am. **125** (2009) 915–921.